

## 2 High-Pressure Raman spectroscopy on low albite

3 <sup>a</sup> *Università di Parma, Dipartimento di Fisica e Scienze della Terra, Parco Area delle Scienze 7/A, 43124 Parma, Italy.*

4 <sup>b</sup> *Università degli Studi di Milano, Dipartimento di Scienze della Terra, via Botticelli 23, 20133 Milano, Italy.*

5 Corresponding author: E-mail: [irene.aliatis@difest.unipr.it](mailto:irene.aliatis@difest.unipr.it); +39 0521 905238

### 7 Abstract

8 The pressure-dependence of the Raman spectrum of low albite, NaAlSi<sub>3</sub>O<sub>8</sub>, has been investigated from 0.0001 to 10.4  
9 GPa, at room temperature, on a single crystal compressed hydrostatically in a diamond-anvil cell. The Raman  
10 vibrational features move to higher wavenumbers  $\nu_i$  with increasing pressure, due to the decrease of the unit-cell  
11 volume corresponding to a drastic shrinkage of the framework. The slopes  $\Delta\nu_i/\Delta P$  of the four investigated bending  
12 modes (*i.e.*, at 478, 507, 578 and 815 cm<sup>-1</sup>, at 0.0001 GPa) show evident changes at ~6.5 GPa and at ~8.5 GPa. This  
13 behaviour may be ascribed, in the absence of phase transitions, to the evolution of the compressional mechanisms at the  
14 atomic scale found in previous high-pressure studies on albite (mainly by X-ray diffraction), through a model based on  
15 tilts of rigid tetrahedra. The Raman data of this study allowed also to bracket the pressure range in which the occurrence  
16 of the first change in the compressional behaviour was found by X-ray diffraction. A comparative analysis between the  
17 main *P*-induced deformation mechanisms, based on previous X-ray structure investigations, and the present Raman  
18 results is carried out.

19  
20 **Keywords** Feldspars, low albite, high-pressure Raman spectroscopy, compressional behaviour.

### 22 Acknowledgments

23 This work was supported by the Italian Ministry of Education (MIUR), grant numbers 2010EARRRZ\_005 and  
24 2008SPZ743 which is gratefully acknowledged. We also acknowledge the generous support to the discussion of R. J.  
25 Angel.

### 27 Introduction

28 The compressional behaviour of feldspars has been deeply studied in order to understand the mechanisms that control  
29 the elastic properties of this abundant class of minerals of the Earth's crust (~ 60 wt%) (*e.g.* Angel 1992; Daniel et al.  
30 1995; Daniel et al. 1997; Downs et al. 1999; Angel 2004; Benusa et al. 2005; Angel et al. 2012; Angel et al. 2013). The  
31 pressure range over which feldspars are thermodynamically stable is limited to 1 GPa in geological environments  
32 (Downs et al. 1994; Benusa et al. 2005; Carpenter 2006), and they become metastable at higher pressures. Nevertheless,  
33 compressional studies at high pressures are needed to provide more accurate data on the thermodynamic properties of  
34 these minerals, and to interpret the deformation changes in the framework, eventually leading to amorphization and to

35 diaplectic glasses with feldspathic composition, as maskelenyte, which are commonly found in natural meteorites  
36 (Velde et al. 1989; Fritz et al. 2005).

37 Feldspars are significantly stiffer than other open-framework silicates, such as quartz (Angel et al. 1997) or zeolites  
38 (Gatta and Lee 2014) but, among rock-forming minerals, they are softer than other rock-forming silicate, *e.g.* olivine  
39 and pyroxenes (Angel 2004). Among natural feldspars, the thermoelastic behaviour of low albite (ideally  $\text{NaAlSi}_3\text{O}_8$ )  
40 has deserved special attention: low albite shows significantly higher thermal expansion than other plagioclases, almost  
41 twice than anorthite (Tribaudino et al. 2010), lower Einstein temperature and more anisotropic thermal deformation  
42 (Tribaudino et al. 2011). Moreover, the unit-cell volume of albite shows a non-linear trend at almost any temperature,  
43 unlike other plagioclases (Tribaudino et al. 2010; Tribaudino et al. 2011). At high pressure, recent determinations of the  
44 equation of state (EoS) of plagioclases (Angel 2004) revealed that low albite shows unusual features (Downs et al.  
45 1994; Benusa et al. 2005): it remains triclinic with  $C\bar{1}$  symmetry at least up to 9.4 GPa and no phase transition occurs  
46 (Benusa et al. 2005), although the unit-cell volume and axial parameters *vs.*  $P$  show a change at  $P > 4$  GPa, ascribable to  
47 a change of the compressional mechanisms at the atomic scale. The first  $P$ -derivative of the bulk modulus, obtained by  
48 an isothermal Birch-Murnaghan EoS fit (Birch 1966), has values  $K' = \partial K/\partial P > 4$  below 4 GPa, whereas at higher  
49 pressure  $K' < 4$ , as observed in the anorthite-richer plagioclases (with An content higher than 30%, Angel 2004). The  
50 closing-up of the crankshaft chains is the dominant compression mechanism and is responsible for the extreme  
51 anisotropy of compression that is typical for all feldspars (Angel et al. 1988; Angel 2004). Albite reveals a more  
52 complex behaviour than other feldspars (Benusa et al. 2005). Two secondary compressional mechanisms act at different  
53 pressures: i) below 4 GPa, the closing-up of the crankshaft chains is the major mechanism, without rotation of  $T_1$   
54 tetrahedra, in addition to the shear of four-membered rings; ii) above 4-5 GPa,  $T_1$  tetrahedra rotate around [001]  
55 direction and albite becomes softer, similarly to what is observed in plagioclase at lower pressures (Angel 2004); iii)  
56 above 8 GPa, a severe softening of the structure as a whole occurs, coupled with an expansion along some directions  
57 (*e.g.*, [110]). At  $P > 8$  GPa, the smallest T-O<sub>c</sub>(o)-T angle decreases to a value of  $\sim 113^\circ$ , which represents an extreme  
58 limit for Al-O-Si bonds, because it enables a Al-Si distance of  $\sim 2.8$  Å (Benusa et al. 2005). Calculation of the strain  
59 tensor (Ohashi and Burnham 1973) from the unit-cell parameters showed that the direction of maximum compression is  
60 close to the (100) plane normal, *i.e.*, along the extension direction of the crankshaft chains, and that this direction  
61 accommodates about the 65% of the volume compression of the framework.

62  
63 In this paper, the results of an in-situ high-pressure Raman spectroscopic study on a single-crystal of low albite are  
64 reported, in order to describe the high-pressure vibrational behaviour of this feldspar, compared with its elastic  
65 properties as determined by in-situ high-pressure X-ray diffraction experiments (Downs et al. 1994; Benusa et al. 2005).  
66 As far as we know, this is the first experiment in which the evolution of the single-crystal Raman spectrum of albite  
67 with pressure is reported.

68

## 69 **Experimental method**

70 The high-pressure Raman spectroscopy experiment was performed on a single crystal of low albite from Minas Gerais  
71 (Brazil) [ $a = 8.1395(5)$  Å,  $b = 12.7838(7)$  Å,  $c = 7.1597(6)$  Å,  $\alpha = 94.242(6)^\circ$ ,  $\beta = 116.590(7)^\circ$ ,  $\gamma = 87.674(5)^\circ$ ,  $V =$   
72  $664.35(9)$  Å<sup>3</sup>, space group  $C\bar{1}$ ]. EPMA-EDS indicate an almost end-member composition, with K<sub>2</sub>O and CaO

73 concentrations of 0.32 and 0.19 wt%, respectively. Further details pertaining to the crystal-chemical characterization of  
74 the sample (*e.g.*, chemical analysis protocol, unit-cell parameters measurement and single-crystal structure refinement  
75 procedure) can be found in Aliatis et al. (2015).

76 An ETH-type diamond anvil cell (DAC), designed by Miletich et al. (2000), was used for the high-pressure Raman  
77 experiment. Stainless-steel T301 foil, 250  $\mu\text{m}$  thick, pre-indented to a thickness of about 100  $\mu\text{m}$  and with a 300  $\mu\text{m}$   
78 hole obtained by electro-spark erosion, was used as a gasket. Type-II diamonds were used as anvils (culet diameter: 600  
79  $\mu\text{m}$ ). A single crystal of low albite ( $120 \times 100 \times 20 \mu\text{m}^3$ ) was placed in the gasket hole along with some ruby chips for  
80 pressure measurements by the ruby-fluorescence method (precision of  $\pm 0.05$  GPa) (Mao et al. 1986). Methanol:ethanol  
81 = 4:1 mixture was used as hydrostatic pressure-transmitting fluid (Angel et al. 2007).

82 Raman spectra were collected in the pressure range 0.0001 - 10.4(5) GPa (16 measurements in compression and 6 in  
83 decompression) using an Olympus BX40 microscope attached to a Jobin Yvon Horiba LabRam confocal Raman  
84 spectrometer, equipped with a charge-coupled detector (CCD). The sample was excited by a continuous-wave single  
85 frequency Nd:YAG blue laser at 473.1 nm end-pumped by a laser diode. The laser beam was focused on the sample  
86 with a spot diameter of nearly 1  $\mu\text{m}$  (50x ultra long working distance objective, NA = 0.55), using a confocal aperture  
87 of 150  $\mu\text{m}$ . The spectral resolution was about 3.5  $\text{cm}^{-1}$ . Unpolarized Raman spectra were collected in backscattered  
88 geometry in the spectral range 100-2000  $\text{cm}^{-1}$ , with 60-90 s counting times and 6-10 accumulations.

89 The (010) cleavage face of the albite crystal was set as much as possible parallel to the culet face of the anvil. The same  
90 configuration was maintained for all the spectra. Before each measurement of the Raman spectrum of the sample and of  
91 the fluorescence spectrum of ruby, the spectrometer was calibrated using the emission lines of a spectroscopic Zn lamp  
92 in the two different spectral ranges. In addition, all spectra were collected at least 20 min after increasing the pressure.  
93 The positions of the Raman bands were determined, with accuracy better than 0.5  $\text{cm}^{-1}$ , after a polynomial baseline  
94 subtraction, by pseudo-Voigt deconvolution procedure (LABSPEC 5.78.24 software package, Jobin Yvon Horiba).

95

## 96 **Results**

97 Some representative Raman spectra of low albite collected in compression and decompression mode are shown in Fig.  
98 1. Twenty-five modes, out of the 39  $A_g$  modes expected by factor group analysis (Aliatis et al. 2015) were observed  
99 with the sample inside the DAC. The useful data were in the spectral range up to 850  $\text{cm}^{-1}$ , due to the intense Raman  
100 bands at 880 and 1000  $\text{cm}^{-1}$  of the pressure-fluid (*i.e.*, methanol or ethanol) and to the strong diamond peak at 1332  
101  $\text{cm}^{-1}$ . At high pressure a general deterioration of the Raman signal due to band overlapping was observed. As an  
102 example, the characteristic peaks at 478 and 507  $\text{cm}^{-1}$  become a single unresolved band at  $P > 8$  GPa, but they split  
103 again in decompression.

104 The major features of the Raman spectra collected at room conditions are preserved up to the highest pressure, with no  
105 evidence of amorphization effects. Some of the weakest Raman bands of low albite disappear with increasing pressure,  
106 especially at low wavenumbers: the number of the observable Raman modes below 250  $\text{cm}^{-1}$  decreases from 7 to 4 at  
107 2.9 GPa, and the  $P$ -evolution of the Raman features in this spectral range cannot be determined unambiguously.

108 A shift towards higher wavenumbers is observed for all Raman modes during compression, an effect completely  
109 reversible in decompression. The distances between the building units forming the albite framework (*i.e.*, Si or Al  
110 tetrahedra) decrease with increasing pressure and the stronger electrostatic repulsion causes the observed blue-shifts.

111 In the following, the wavenumbers used to label the investigated Raman bands are those found in the Raman spectrum  
112 at room  $T$ ,  $P$ . The pressure-induced evolution of six selected (well observable) Raman bands at 149-290-48-507-578-  
113 815  $\text{cm}^{-1}$ , along with the linear fits to their  $\nu_i(P)$  curves, are shown in Fig. 2. The wavenumber blue shifts, within the full  
114  $P$ -range investigated, are:  $\Delta\nu_{149} = 26.0 \text{ cm}^{-1}$ ,  $\Delta\nu_{290} = 15.7 \text{ cm}^{-1}$ ,  $\Delta\nu_{478} = 29.1 \text{ cm}^{-1}$ ,  $\Delta\nu_{507} = 16.2 \text{ cm}^{-1}$ ,  $\Delta\nu_{578} = 4.2 \text{ cm}^{-1}$ ,  
115 and  $\Delta\nu_{815} = 17.3 \text{ cm}^{-1}$ .

116 Excluding the Raman band at 149  $\text{cm}^{-1}$ , which displays a constant  $\Delta\nu/\Delta P$  slope over the entire  $P$ -range, variations of the  
117  $\Delta\nu_i/\Delta P$  slopes are observed for the studied modes (see Table 1). This suggests different compressional mechanisms for  
118 the building units involved in each mode. The modes involving mainly Na (*e.g.*, 149  $\text{cm}^{-1}$ , Aliatis et al 2015) show the  
119 most pronounced changes in slope with pressure, consistent with the clue that Na atoms are just ‘pushed around’ by the  
120 framework and that the cavity is rapidly compressed. A common feature of the  $\nu_i(P)$  curves is an apparent discontinuity  
121 at  $\sim 6.5$  GPa. Raman data suggest, therefore, that the internal structural rearrangements occur in a sharp pressure  
122 interval, at about 6.5 GPa and not spread out from 4 to 8 GPa as suggested by previous X-rays studies on elasticity  
123 (Benusa et al. 2005). This behaviour cannot be ascribed to a phase transition (as it can be ruled out on the basis of the  
124 X-ray data), it is rather the effect of a change in the compressional mechanisms at the atomic scale, with a resulting  
125 change of the elastic behaviour. In addition, whereas most modes evolve smoothly for  $P > 7$  GPa, the high-frequency  
126 mode at 815  $\text{cm}^{-1}$  shows another discontinuity in  $\nu_{815}(P)$  at  $P \sim 8.5$  GPa.

127

## 128 Discussion

129 Interesting correspondences can be found if the in-situ high-pressure Raman results here reported and the structural data  
130 from literature are compared. Looking at the pressure-evolution of the T-O-T bond angles and of the O-O-O ring  
131 angles, based on the structure refinements, as given by Benusa et al. (2005), a discontinuity at  $P \sim 6$  GPa is detected. In  
132 particular, the most evident structural rearrangement reflects the reduction in the T-O<sub>B</sub>(o)-T and T-O<sub>C</sub>(o)-T bond angles,  
133 which results in the closing-up of the crankshaft chains and in the shear of the four-membered rings of tetrahedra. The  
134 shear causes the narrowing of the channels which is responsible of the softness along the (100) plane normal, as  
135 observed in all feldspars (Downs et al. 1994; Angel 2004; Benusa et al. 2005). Angel et al. (2012) showed that all the  
136 essential features of the structures (*i.e.*, unit-cell parameters and volumes, their expansion and compression induced by  
137 changes in pressure, temperature, and composition) are generated by tetrahedral tilting, and that the fundamental reason  
138 for feldspars anisotropy lies in the topology of the tetrahedral framework. In particular, four tilts are allowed in a ring of  
139 four corner-linked tetrahedra with point symmetry 2: #1 the rotation of T<sub>1</sub> tetrahedra around the O<sub>B</sub>-O<sub>D</sub> edge; #2  
140 rotation of T<sub>2</sub> tetrahedra around the O<sub>B</sub>-O<sub>D</sub> edge; #3 mutual rotation of the T<sub>2</sub> by equal but opposite amounts around  $a^*$ ;  
141 #4 shear of the ring within the (010) plane. In triclinic feldspars, there are four non-equivalent tetrahedra, so four  
142 individual tilts of the tetrahedra with respect to the ring: tilt #1 will be split in T<sub>1</sub>(o) and T<sub>1</sub>(m) tilts, and tilt #2 in T<sub>2</sub>(o)  
143 and T<sub>2</sub>(m) tilts. The O-O repulsions control the values of these tilts and, therefore, the anisotropy of the structure,  
144 because tilts maximize the shortest O-O distances in the structure (Angel et al. 2012; Angel et al. 2013). Therefore,  
145 considering the structural changes in terms of tilts of rigid tetrahedra, the variation in the tilting angles are expected to

146 be relate especially with the framework bending modes (*i.e.*, the Raman modes at 478, 507, 578 and 815  $\text{cm}^{-1}$ , Aliatis et  
147 al. 2015).

148 The pressure-induced evolution of tilt angles in triclinic structures is shown in Fig. 3. They have been recalculated from  
149 the experimental data of Benusa et al. (2005) and Downs et al. (1994), using the definition and the calculations reported  
150 in Angel et al. (2012). It is evident that the rate in the variation of all tilts changes significantly at 6 GPa, in good  
151 agreement with our Raman data of this study. In Fig. 4, the correlation between the change in O-O-O angles and tilt #4  
152 (*i.e.*, shear of the ring) is shown. Tilts do not include the internal deformation of the tetrahedra, because they are only a  
153 measure of the response of the structure interpreted in terms of non-deformable tetrahedra, so they do not explain the  
154 further change at  $P > 8.5$  GPa.

155 The Raman mode at 478  $\text{cm}^{-1}$  shows the most pronounced Raman shift between 0.0001 and 6.5 GPa ( $\Delta\nu_{478} = 29.1 \text{ cm}^{-1}$ ,  
156 Table 1). Comparing the vibrational patterns corresponding to the Raman features at 478, 507, 578 and 815  $\text{cm}^{-1}$ , it  
157 appears, especially in the *ab* projection (Fig. 5), that the mode at 478  $\text{cm}^{-1}$  squeezes the cage inwards, whereas the  
158 modes at higher wavenumbers stretch the cage outwards. Changes in T-O-T and O-O-O angles result in the narrowing  
159 of the tetrahedral cages, which causes an increase in the Coulomb repulsion between atoms: the atomic pattern of the  
160 mode at 478  $\text{cm}^{-1}$  may explain its largest wavenumber increase with pressure.

161 At  $P > 6.5$  GPa, the Raman band at 507  $\text{cm}^{-1}$  exhibits the steepest  $\Delta\nu/\Delta P$  and the slope of the 578  $\text{cm}^{-1}$  mode changes its  
162 sign (see Table 1), suggesting a relevant structural rearrangement.

163 In addition to the 6.5 GPa discontinuity, the mode at 815  $\text{cm}^{-1}$  shows a further abrupt change in  $\Delta\nu/\Delta P$  at about 8.5 GPa.  
164 As reported in Aliatis et al. (2015), this mode has a significant contribution from Si-O stretching vibrations and may be  
165 affected by variation of the internal geometry of the  $\text{TO}_4$  tetrahedra. The discontinuity at 8.5 GPa could mirror the  
166 severe softening of the structure observed at  $P > 8$  GPa by Benusa et al. (2005).

167 The discontinuity at 6.5 GPa may be noticed, even if at a lesser extent, also by the Raman mode at 290  $\text{cm}^{-1}$ , which  
168 consists mainly of rotations of the tetrahedra (Aliatis et al. 2015).

169 The wavenumber of the Raman mode at  $\sim 149 \text{ cm}^{-1}$  changes linearly over the entire investigated pressure range. This  
170 mode is related mostly to the Na atoms vibrations, in particular to Na translations within the tetrahedral cage (Aliatis et  
171 al. 2015). As the Na atoms are just 'pushed around' (Downs et al. 1994; Benusa et al. 2005), and the cavity tends to be  
172 rapidly compressed, a significant change with pressure is expected. Na atom does not change its coordination number  
173 within the *P*-range investigated, despite the significant decrease in the Na-O distances; this in contrast to microcline,  
174 where the K site increases its coordination number by bonding the additional  $\text{O}_{\text{B(m)}}$  atom as the framework is  
175 compressed (Downs et al. 1999). In this respect, the behaviour of the extra-framework population with increasing  
176 pressure in albite is similar to that observed in other open-framework silicates (*e.g.*, some zeolites or feldspathoids,  
177 Gatta 2008; Gatta 2010; Gatta and Lotti 2016).

178 Changes in peak linewidth are not significant (*i.e.*, maximum increase of about 2-2.5  $\text{cm}^{-1}$  in the investigated pressure  
179 range), confirming that the experiment was conducted under hydrostatic conditions and no evidence of *P*-induced  
180 amorphization occurs up to the maximum pressure achieved.

181

182 **Conclusions**

183 To the best of our knowledge, this is the first study in which the evolution of the Raman active modes of low albite has  
184 been investigated by an in-situ experiment up to 10.4 GPa. Our experimental findings can be summarized as follows:  
185 the six investigated Raman modes (*i.e.*, 149, 290, 478, 507, 578, 815  $\text{cm}^{-1}$  at 0.0001 GPa) show a smooth evolution  
186 (stiffening) from room pressure to about 6 GPa and, excluding the mode involving Na atoms (*i.e.*, 149  $\text{cm}^{-1}$ ), a  
187 significant change in their vibrational behaviour occurs at  $P \sim 6.5$  GPa: this allows localizing the first change in the  
188 compressional behaviour of albite previously found by X-ray diffraction in a large  $P$  range (*i.e.*, 4-8 GPa). A further  
189 change at about 8.5 GPa of the mode at 815  $\text{cm}^{-1}$  confirms a second rearrangement of the structure, including the  
190 compression and severe distortion of the tetrahedra, observed by X-ray diffraction at  $P > 8$  GPa.

191 **References**

- 192 Aliatis I, Lambruschi E, Mantovani L, Bersani D, Andò S, Gatta GD, Gentile P, Salvioli-Mariani E, Prencipe M,  
193 Tribaudino M, Lottici PP (2015) A comparison between ab initio calculated and measured Raman spectrum of  
194 triclinic albite (NaAlSi<sub>3</sub>O<sub>8</sub>). *J Raman Spectrosc* 46: 501–508
- 195 Angel RJ (1992) Order-disorder and the high-pressure P1-I1 transition in anorthite. *Am Mineral* 77:923–929.
- 196 Angel RJ (2004) Equations of state of Plagioclase Feldspars. *Contrib to Mineral Petrol* 146:506–512.
- 197 Angel RJ, Allan DR, Miletich R, Finger LW (1997) The use of quartz as an internal pressure standard in high-pressure  
198 crystallography. *J Appl Crystallogr* 30:461–466.
- 199 Angel RJ, Bujak M, Zhao J, Gatta GD, Jacobsen SD (2007) Effective hydrostatic limits of pressure media for high-  
200 pressure crystallographic studies. *J Appl Crystallogr* 40:26–32.
- 201 Angel RJ, Hazen RM, McCormick TC, Prewitt CT, Smith JR (1988) Comparative compressibility of end-member  
202 feldspars. *Phys Chem Miner* 15:313–318.
- 203 Angel RJ, Ross NL, Zhao J, Sochalski-Kolbus LM, Kruger H, Schmidt BC (2013) Structural controls on the anisotropy  
204 of tetrahedral framework: the example of monoclinic feldspars. *Eur J Mineral* 25:597–614.
- 205 Angel RJ, Sochalski-Kolbus LM, Tribaudino M (2012) Tilts and tetrahedra: The origin of the anisotropy of feldspars.  
206 *Am Mineral* 97:765–778.
- 207 Benusa MD, Angel RJ, Ross NL (2005) Compression of albite, NaAlSi<sub>3</sub>O<sub>8</sub>. *Am Mineral* 90:1115–1120.
- 208 Birch F (1966) Compressibility, elastic constants. In: Clark SP (ed) *Handbook of physical constants*. Geol. Soc. Am.  
209 *Mem.*, pp 97–174
- 210 Carpenter MA (2006) Elastic properties of minerals and the influence of phase transitions. *American Mineralogist*  
211 91:229–246.
- 212 Daniel I, Gillet P, Ghose S (1995) A new high-pressure phase transition in anorthite (CaAl<sub>2</sub>Si<sub>2</sub>O<sub>8</sub>) revealed by Raman  
213 spectroscopy. *Am Mineral* 80:645–648.
- 214 Daniel I, Gillet P, McMillan PF, Wolf G, Verhelst MA (1997) High-pressure behavior of anorthite: Compression and  
215 amorphization. *J Geophys Res* 102:10313.
- 216 Downs RT, Hazen RM, Finger LW (1994) The high-pressure crystal chemistry of low albite and the origin of the  
217 pressure dependency of Al-Si ordering. *Am Mineral* 79:1042–1052.
- 218 Downs RT, Yang H, Hazen RM, Finger LW, Prewitt CT (1999) Compressibility mechanisms of alkali feldspars:  
219 New data from reedmergnerite. *Am Mineral* 84:333–340.
- 220 Fritz J, Greshake A, Stoffler D (2005) Micro-Raman spectroscopy of plagioclase and maskelynite in Martian  
221 meteorites: evidence of progressive shock metamorphism. *Antarct Meteorite Res* 18:96–116.

- 222 Gatta GD (2008) Does porous mean soft? On the elastic behaviour and structural evolution of zeolites under pressure. *Z*  
223 *Kristallogr* 223:160–170.
- 224 Gatta GD (2010) Extreme deformation mechanisms in open-framework silicates at high-pressure: Evidence of  
225 anomalous inter-tetrahedral angles. *Micropor Mesopor Mater* 128:78–84.
- 226 Gatta GD, Lee Y (2014) Zeolites at high pressure: A review. *Min Mag* 78:267–291.
- 227 Gatta GD., Lotti P (2016) Cancrinite-group minerals: Crystal-chemical description and properties under non-ambient  
228 conditions - A review. *Am Mineral* 101:253–265.
- 229 Mao HK, Xu J, Bell PM (1986) Calibration of the ruby pressure gauge to 800 kbar under quasi-hydrostatic conditions. *J*  
230 *Geophys Res* 91:4673.
- 231 Miletich R, Allan DR, Kuhs WF (2000) High-pressure single crystal techniques. In: Hazen RM, Downs RT (eds) High-  
232 temperature and high-pressure crystal chemistry. *Reviews in Mineralogy and Geochemistry*. pp 445–519
- 233 Ohashi Y, Burnham CW (1973) Clinopyroxene Lattice Deformations: The Roles of Chemical Substitution and  
234 Temperature. *Am Mineral* 58:843–849.
- 235 Tribaudino M, Angel RJ, Cámara F, Nestola F, Pasqual D, Margiolaki I (2010) Thermal expansion of plagioclase  
236 feldspars. *Contrib to Mineral Petrol* 160:899–908.
- 237 Tribaudino M, Bruno M, Nestola F, Pasqual D, Angel RJ (2011) Thermoelastic and thermodynamic properties of  
238 plagioclase feldspars from thermal expansion measurements. *Am Mineral* 96:992–1002.
- 239 Velde B, Syono Y, Kikuchi M, Boyer H (1989) Raman microprobe study of synthetic diaplectic plagioclase feldspars.  
240 *Phys Chem Miner* 16:436–441.
- 241



242 **Tables**

243

244 **Table 1** Raman shifts as a function of pressure for six selected Raman modes

245

<b>Modes</b> (cm <sup>-1</sup> )	$ \Delta\nu _{0-10.4 \text{ GPa}}$ (cm <sup>-1</sup> )	$P < 6.5 \text{ GPa}$		$P > 6.5 \text{ GPa}$		$P > 8.5 \text{ GPa}$	
		$\Delta\nu/\Delta P$ (cm <sup>-1</sup> GPa <sup>-1</sup> )	uncertainties (cm <sup>-1</sup> GPa <sup>-1</sup> )	$\Delta\nu/\Delta P$ (cm <sup>-1</sup> GPa <sup>-1</sup> )	uncertainties (cm <sup>-1</sup> GPa <sup>-1</sup> )	$\Delta\nu/\Delta P$ (cm <sup>-1</sup> GPa <sup>-1</sup> )	uncertainties (cm <sup>-1</sup> GPa <sup>-1</sup> )
149	26.0	2.7	0.1				
290	15.7	1.9	0.1	1.3	0.1		
478	29.1	3.6	0.1	1.9	0.3		
507	16.2	1.1	0.1	2.9	0.2		
578	4.2	1.8	0.1	-1.4	0.2		
815	17.3	2.2	0.1	-0.5	0.5	3.1	0.4

246

247 **Caption of the Figures**

248

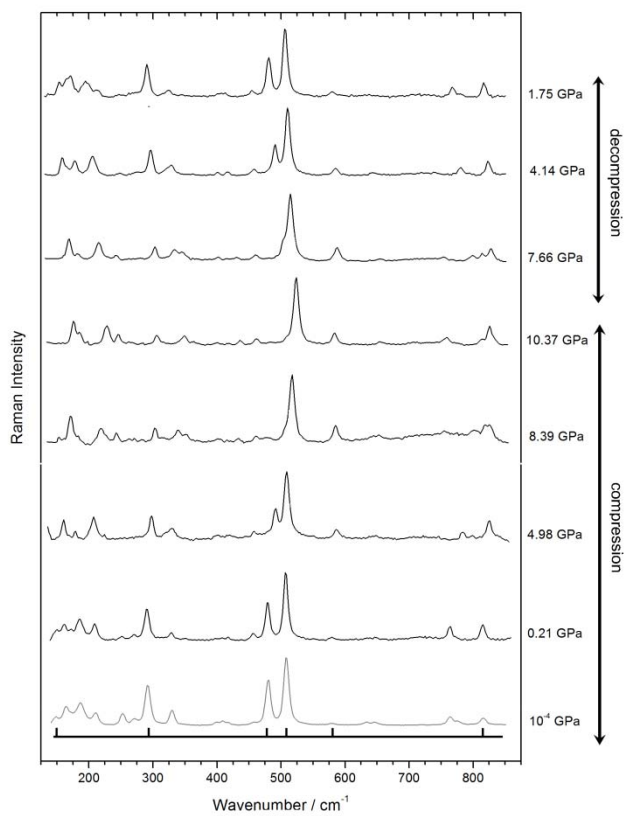
249 **Fig. 1** Pressure-evolution of the Raman spectrum of low albite during isothermal ( $T = 25\text{ °C}$ ) compression and  
250 decompression, from 0.0001 to 10.4 GPa. The spectrum at 0.0001 GPa was collected with the crystal in air

251 **Fig. 2** Pressure-evolution of some selected Raman bands. Full and empty symbols correspond to the compression and  
252 decompression experiments, respectively. Lines are least square fits to data, to use as guide to the eye

253 **Fig. 3** Plots of the four possible tilts in the alkali-feldspar structure as a function of pressure. Tilts have been defined  
254 and calculated according to Angel et al. (2012). Data from the refinements of Benusa et al. (2005) and the lower- $P$   
255 refinements by Downs et al. (1994)

256 **Fig. 4** The shear of the four-membered ring of tetrahedra. O-O-O angles from Benusa et al. (2005); tilt #4 is defined in  
257 Angel et al. (2012), along with the protocol for its calculation. Lines are drawn as guide to the eye

258 **Fig. 5** Vibrational patterns of the modes corresponding to the Raman bands at 478, 507, 578 and 815  $\text{cm}^{-1}$ , projected on  
259 the  $ab$  plane. Wavenumbers refer to room  $T,P$ . Calculated atomic displacements are indicated as black arrows. Atom  
260 types are: Na (yellow), Si (red), Al (green) and O (blue)



262

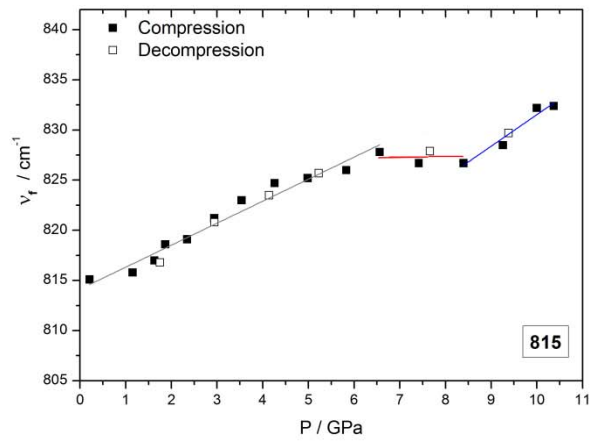
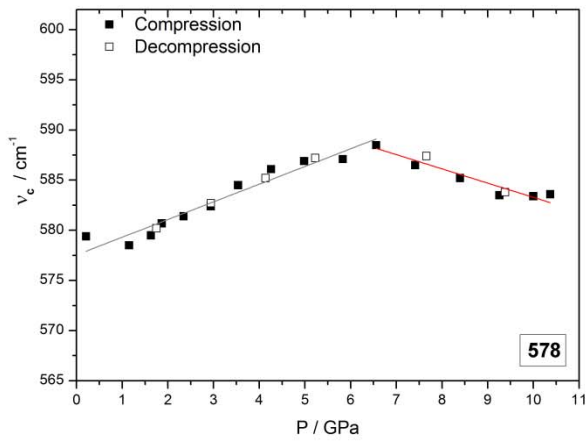
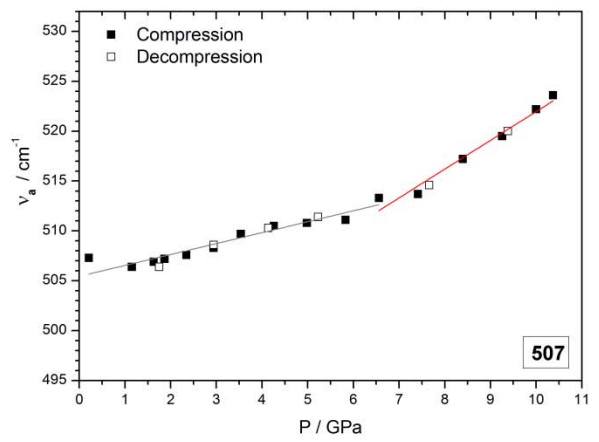
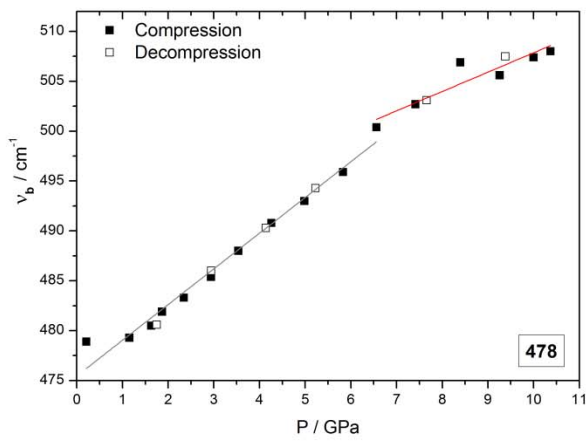
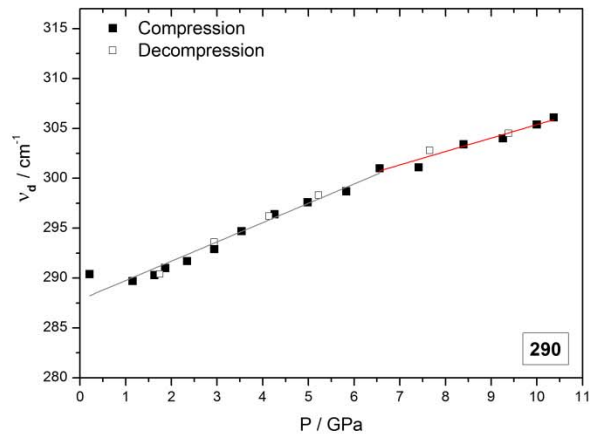
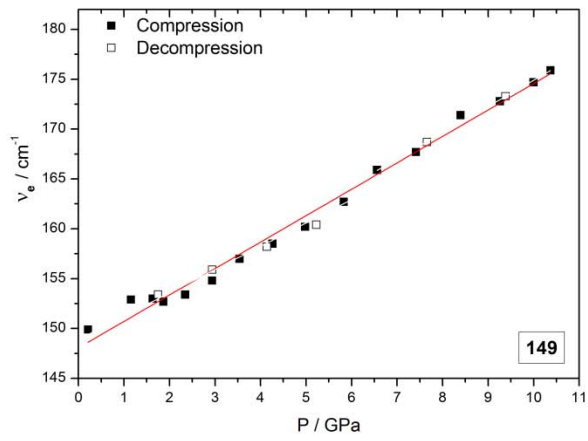
263

Fig1.tiff

264

Graphics program: Origin Pro8

265



266

267

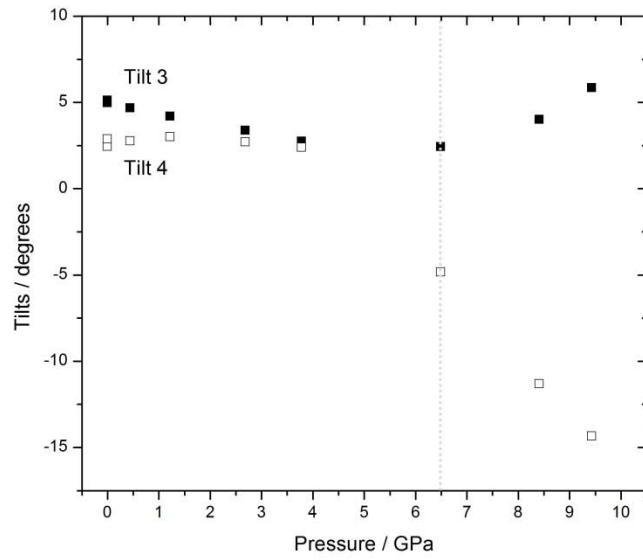
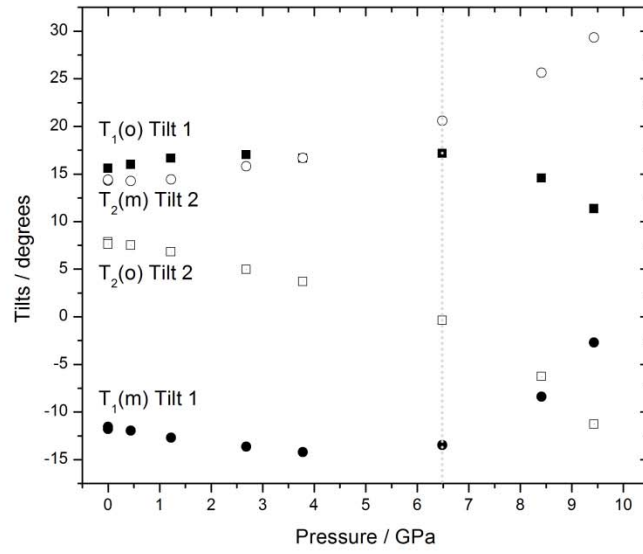
268

269

270

Fig2.tiff

Graphics program: Origin Pro8



271

272

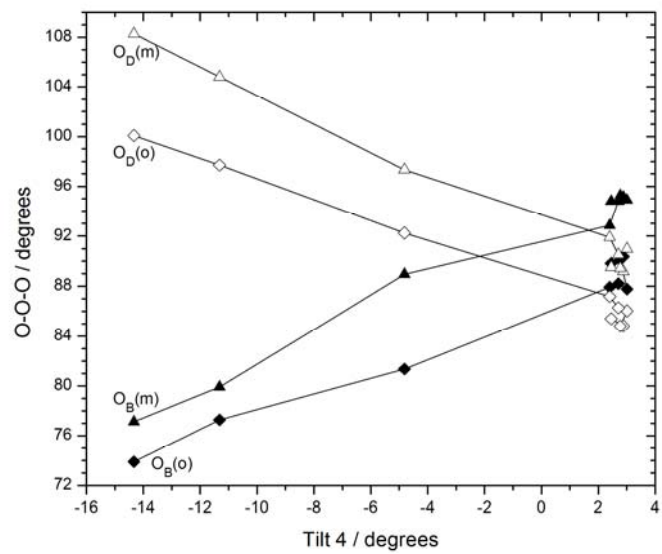
Fig3.tiff

273

Graphics program: Origin Pro8

274

275



276

277

Fig4.tiff

278

Graphics program: Origin Pro8

279

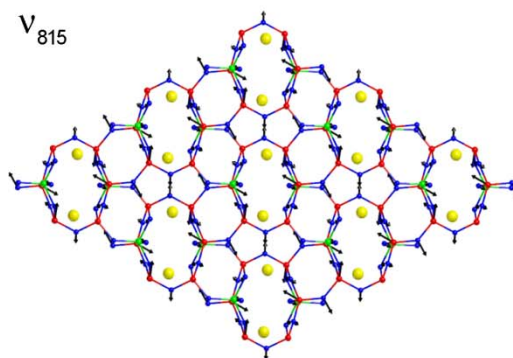
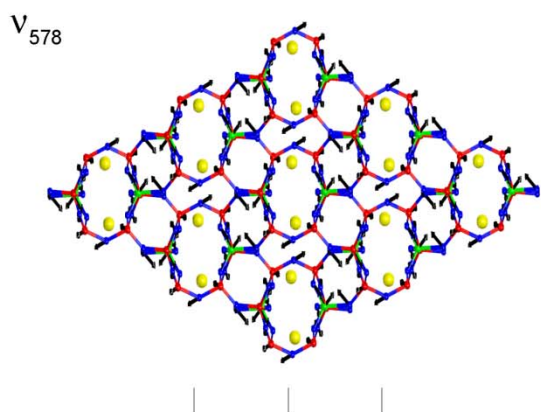
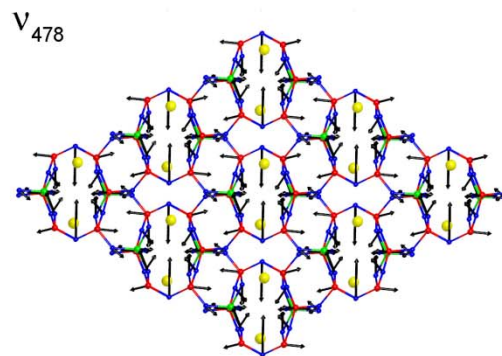
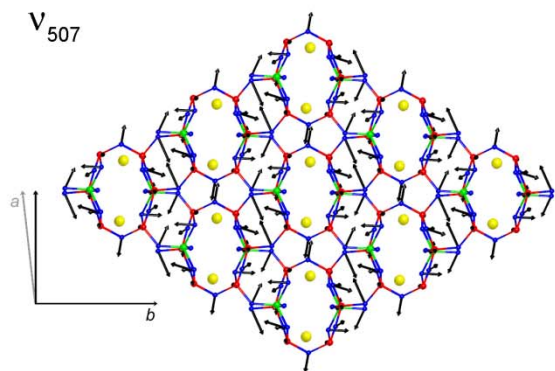
280

281

282

283

284



285

286

Fig5.tiff

287

Graphics program: Moldraw software (<http://www.moldraw.unito.it>)

288

289

290